IEEE Access
Multidisciplinary ⋮ Rapid Review ⋮ Open Access Journal

Received February 26, 2018, accepted May 12, 2018, date of publication May 22, 2018, date of current version June 19, 2018.

Digital Object Identifier 10.1109/ACCESS.2018.2837355

Bandpass Impedance Transformers With Extremely High Transforming Ratios Using Π-Tapped Feeds

CHI-WEN HSIEH, (Member, IEEE), SHIH-CHENG LIN, (Member, IEEE), AND JIA-YING LI
Department of Electrical Engineering, National Chiayi University, Chiayi 60004, Taiwan

Corresponding author: Shih-Cheng Lin (sclin@mail.ncyu.edu.tw)

This work was supported by the National Science Council of Taiwan under Grant MOST 105-2221-E-415-002, Grant MOST 106-2221-E-415-002, Grant MOST 105-2923-E-194-004-MY3, and Grant MOST 107-NU-E-415-001-NU.

ABSTRACT Bandpass impedance transformers (BPIMTs) with extremely high transforming ratios by adopting the proposed Π-tapped feeds are realized in this paper. Π-tapped feeds composed of two shunt stubs and one-section line performing the impedance transforming function are introduced. To validate the generality of the proposed approach, two different types of bandpass transformers, i.e., type-A and type-B adopting a short-ended parallel coupled-line and a via-inductive coupling as their interstage couplings, respectively, originating from two coupled-resonator filter topologies are designed. The synthesis procedures and design formulas of the two transformer types are provided, and the auxiliary graphs for different impedance transforming ratios are thoroughly investigated. The circuit-level simulated results of the proposed BPIMTs agree well with the theoretical results calculated from the coupling matrix, thus validating the design approach. Specifically, two type-A prototypes with the transforming ratios of 20 (200 Ω/10 Ω) and 95 (475 Ω/5 Ω), respectively, and one type-B prototype with a transforming ratio of 104 (520 Ω/5 Ω) were demonstrated. The proposed transformer is capable of satisfactorily matching the low and high impedances, and it also possesses the highest impedance transforming ratio ever reported in the literature.

INDEX TERMS Impedance transformer, bandpass function, Π-tapped feed, parallel-coupled line, inductive coupling.

I. INTRODUCTION

In microwave systems, impedance transformers (IMT) play a critical role in impedance matching or maximum power transfer, and they are also widely utilized in power dividers/combiners [1]–[3], baluns [4], [5], power amplifiers [6]–[8], and low-noise amplifiers. Generally, if the IMT is just serving as an impedance transforming connection between components, it is designed for wideband performance [9], [10]. On the other hand, in most microwave communication systems, the filters are usually inserted between the antennas and transceivers and both their I/O ports are commonly matched with system impedance Z_0. The conventional approach of designing antennas is to adjust the dimensions to achieve radiation resistance equal to Z_0. However, different types of antennas may provide significantly different impedance levels resulting from their radiation nature, which is not easy to control to the demanded level, and thus, the IMTs are needed. Therefore, from a system viewpoint, it would be beneficial to combine the impedance transforming and filtering functions into a single component to save circuit size and reduce loss.

Quite a few research studies have been carried out to design IMTs that can be roughly classified into three categories: multi-section IMTs using cascading quarter-wave transmission lines ($\lambda/4$ TLs) [10]–[12], TL-IMT [13], [14], and one-/multi-section parallel coupled-line IMTs [15]–[19]. Concerning [10], through the derivation of the transmission coefficient of a two-port network and equating it with the transfer function of the Chebyshev response, the required electrical parameters can be derived. Once the required impedance ratio is high, the multi-section IMTs [11], [12] using $\lambda/4$ TLs suffer from very wide/narrow line widths that may not be practical in common applications. A single-section coupled line was employed as the impedance-transforming DC block with $r_z = 2$ (50Ω/25Ω) [15]. In addition, the IMT using open-ended parallel-coupled lines (PCLs) with a transforming ratio of 2 (50Ω/25Ω) [17] or based on short-ended PCLs with transforming ratios up to 20 (1000Ω/50Ω) [18] were presented. The open-ended two-section coupled-line IMT proposed in [19] achieved an ultra-high impedance ratio of 10 (50Ω/5Ω). According to these works, it is observed that the IMTs utilizing open-ended PCLs seem more suitable for transforming relatively low source/load impedances [19]. Once the source/load impedances are both relatively high, the strong coupling required may be not achievable due to process limitation. In contrast, the IMT using short-ended PCLs is preferable in transforming relatively high source/load impedances [18]. Finding an approach for dealing with wide-range source/load impedance transformation is an attractive research topic.

The tapped-line feed structure can be traced back to [20], 1979. Due to the simple structure and tight coupling, the tapped-line has been widely adopted in many different types of filters as a feeding structure [21]–[23]. In [24] and [25], efforts are made to improve the feeding characteristics of conventional tapped-line feeds. From the theoretical viewpoint, the conventional tapped feed can be further modified to possess impedance-transforming capability.

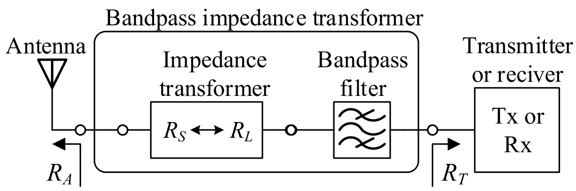

FIGURE 1. Dual functions of the proposed bandpass impedance transformer.

This study was intended to design a dual-function microwave component possessing filtering capability and impedance transformation as shown in Fig. 1. By adopting the proposed Π-tapped feed structures as the I/O feeds of the coupled-resonator structure, impedance transformation and a filtering function can be simultaneously accomplished. In addition, two transmission zeros contributed by the inherent stubs of the Π-tapped feeds can potentially be used to suppress the spurious passbands. Two different types of BPIMT, type-A and type-B, based on the Π-tapped feeds are discussed to show the generality of the proposed design. The circuit-level simulated results and calculations from the coupling matrix show significant agreement in terms of bandwidth, passband ripple, and impedance-matching. Theoretically speaking, the proposed method of designing BPIMT can be used in those coupled-resonator filters using different coupling mechanisms. The BPIMTs are implemented and measured showing satisfactory electrical performance.

II. Π-TAPPED FEEDS WITH IMPEDANCE-TRANSFORMATION FUNCTION

A bandpass impedance transformer (BPIMT) that possesses both the impedance transforming capability and the filtering

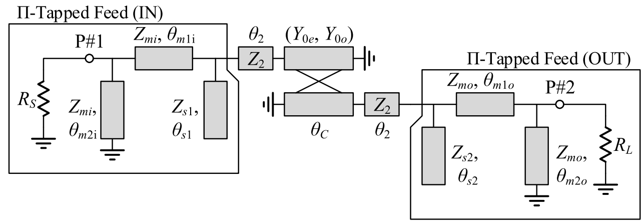

FIGURE 2. Schematic of the proposed type-A filtering impedance transformer with spurious suppression ($Y_{0e} = 1/Z_{0e}$, $Y_{0o} = 1/Z_{0o}$).

function can be designed using the inverter-based coupled-resonator filter [25] through appropriate modification. Fig. 2 depicts the equivalent-circuit of the proposed type-A 2nd-order BPIMT composed of two Π-tapped feeds and one short-ended parallel-coupled line (SE-PCL). The transformer is specified with center frequency f_0, transforming ratio $r_Z = R_L / R_S$, fractional bandwidth Δ, and order $N = 2$ to minimize the insertion loss. The corresponding element values of the lowpass prototype filter are $[g_0, g_1, g_2, g_3]$. The two attached open-ended stubs associated with the I/O Π-tapped feeds can be used for spurious suppression or interference rejection by contributing two transmission zeros.

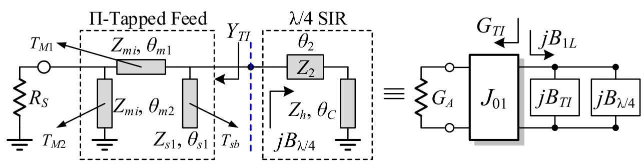

FIGURE 3. Singly loaded resonator fed by the proposed Π-tapped feed for evaluating the external quality factor. ($G_S = 1/R_S$, $Y_{mi} = 1/Z_{mi}$, $Y_h = 1/Z_h$, $Y_2 = 1/Z_2$).

Redrawing the singly loaded resonator composed of the Π-tapped feed and the λ/4 stepped-impedance resonator (SIR) adjacent to the input port in Fig. 3 for the following discussion, the Π-tapped feed exploited in the loaded resonator consists of a shunt short-ended stub T_{M2}, a cascading line section T_{M1} and a shunt open-ended stub T_{sb}. With regard to the SIR, its design parameters are (Y_h, θ_C) and (Y_2, θ_2). As shown in Fig. 3, the input admittance $Y_{TI} = G_{TI} + jB_{TI}$ of the Π-tapped feed must be purely resistive exactly at the operation frequency, whereas its reactive component behaves as a shunt resonator. The derived B_{TI} is expressed as

$$B_{TI} = \frac{Y_{mi}[G_S^2(\sin 2\theta_{A1} - 2\sin 2\theta_{m1}) + (G_S^2 - 4Y_{mi}^2)\sin 2\theta_{A2}]}{8[(G_S \sin\theta_{m1i}\sin\theta_{m2i})^2 + (Y_{mi}\sin\theta_{A2})^2]} + Y_{s1}\tan\theta_{s1}, \quad (1)$$

where $\theta_{A1} = \theta_{m1i} - \theta_{m2i}$, and $\theta_{A2} = \theta_{m1i} + \theta_{m2i}$. For a given source resistance R_S and line impedance Z_{mi}, it is demanded that $B_{TI}(\theta_{m1i}, \theta_{m2i}) = 0$ at f_0 to ensure resonance with the selected stub (Z_{s1}, θ_{s1}). For simplification, B_{TI} can be modeled as a shunt resonator around resonant frequency f_0,

$$B_{TI} = b_{TI}(f/f_0 - f_0/f), \quad (2)$$

where f denotes the frequency variable, and b_{TI} is its susceptance slope parameter. This parasitic resonator and the $\lambda/4$ stepped-impedance resonator (SIR) jointly constitute the overall input resonators $jB_{1L} = j(B_{TI} + B_{\lambda/4})$. Eventually, the total susceptance slope parameter of resonator 1 seen from the left-handed side (LHS) can be acquired by finding the differentiation of B_{1L}.

$$b_{1L} = \frac{f_0}{2}\frac{dB_{TI}}{df} + \frac{f_0}{2}\frac{dB_{\lambda/4}}{df} = b_{TI} + b_{\lambda/4}, \tag{3}$$

where $b_{\lambda/4}$ denotes the susceptance slope parameter of the $\lambda/4$ SIR composed of two sections of transmission lines (Z_h, θ_c) and (Z_2, θ_2) that can be analytically given as

$$b_{\lambda/4} = Y_2 \sec^2\theta_2 \frac{\theta_2(1+\alpha_Y^2\tan^2\theta_1) + \alpha_Y\theta_1\sec^2\theta_1}{2(\alpha_Y\tan\theta_1 + \tan\theta_2)^2}. \tag{4}$$

with $\alpha_Y = Y_2/Y_1$, $\theta_1 = \theta_c$, and $Y_1 = Y_h$.

To meet the filter specifications, the external quality factor of the proposed Π-tapped feed must fulfill the following condition

$$\frac{b_{1L}(\theta_{m1i}, \theta_{m2i})}{G_{TI}(\theta_{m1i}, \theta_{m2i})} = Q_{EI}, \quad \text{where} \quad Q_{EI} = \frac{g_0 g_1}{\Delta}. \tag{5}$$

Using (5), the electrical lengths $(\theta_{m1i}, \theta_{m2i})$ can be solved for. Similarly, the electrical lengths $(\theta_{m1o}, \theta_{m2o})$ of the output feed with predetermined load resistance and line impedance Z_{mo} can be calculated from $B_{TO}(\theta_{m1o}, \theta_{m2o}) = 0$ and $b_{2R}/G_{TO} = Q_{EO}$ seen from the RHS of resonator 2, where $Q_{EO} = g_2 g_3/\Delta$.

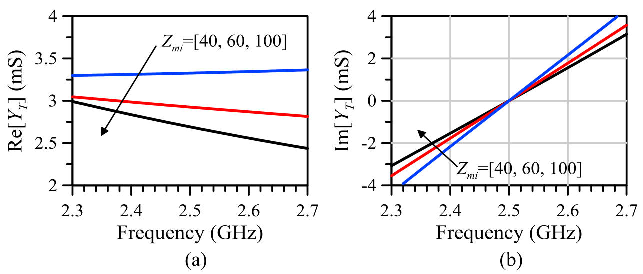

FIGURE 4. Input susceptance Y_{TI} of the proposed Π-tapped feed under $R_S = 10\ \Omega$ and open-ended stub $(Z_{s1}, \theta_{s1}) = (70\Omega, 45°)$. (a) Real part. (b) Imaginary part.

To validate the design guideline, a BPIMT is designed with arbitrary f_0 and $\Delta = 7\%$ for a 0.1-dB-ripple Chebyshev response. The associated values of the lowpass prototype are $[g_0, g_1, g_2, g_3] = [1, 0.8431, 0.6220, 1.3554]$. Using $g_0 = 1$ and $g_1 = 0.8341(Q_{EI} = 12.0443)$, the input admittances Y_{TI} versus frequency of the Π-tapped feeds for $Z_{mi} = 40$, 60, and 100 Ω are accordingly calculated and drawn in Fig. 4. Obviously, the admittance Y_{TI} contributed by the Π-tapped feed behaves like a parallel resonator around f_0 and the equivalent input conductance G_{TI} varies with different characteristic impedance Z_{mi}. By choosing the $\lambda/4$ resonator adjacent to the tapped feed as uniform-impedance ($Z_1 = Z_2 = 60\ \Omega$, $\theta_C = 70°$, $\theta_2 = 20°$), its susceptance slope parameter can be calculated as $b_{\lambda/4} = 1.31$ cS. With the aid of (5), the resultant

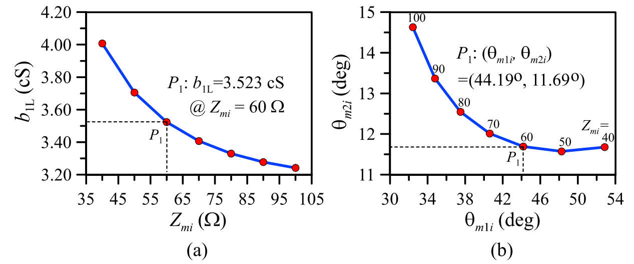

FIGURE 5. (a) Susceptance slope parameter b_{1L} and (b) $(\theta_{m1i}, \theta_{m2i})$ of the proposed Π-tapped feed incorporating $\lambda/4$ SIR under $R_S = 10\ \Omega$ and open-ended stub $(Z_{s1}, \theta_{s1}) = (70\ \Omega, 45°)$.

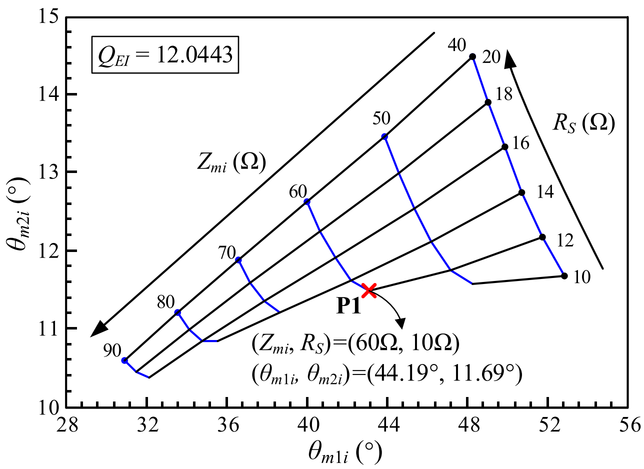

FIGURE 6. Design graph of θ_{m1i} and θ_{m2i} using Z_{mi} and R_S as parameters with termination open-ended stub $(Z_{s1}, \theta_{s1}) = (70\ \Omega, 45°)$.

susceptance slope parameter b_{1L} of resonator 1 seen from the LHS is shown in Fig. 5(a) solved under $R_S = 10\ \Omega$ and open-ended stub $(Z_{s1}, \theta_{s1}) = (70\ \Omega, 45°)$. Moreover, the auxiliary chart of $(\theta_{m1i}, \theta_{m2i})$ with different Z_{mi} is illustrated in Fig. 5(b).

For convenience, a low-Z (R_S) to high-Z (R_L) transformation is considered. In Fig. 6, the design graphs are shown for determining the $(\theta_{m1i}, \theta_{m2i})$ using both Z_{mi} and $10\ \Omega \le R_S \le 20\Omega$ as parameters with the attached open-ended stub $(Z_{s1}, \theta_{s1}) = (70\ \Omega, 45°)$. For ease of usage, only monotonic solutions of $(\theta_{m1i}, \theta_{m2i})$ (as R_S increases, θ_{m1i} increases and θ_{m2i} decreases; as Z_{mi} increases, both θ_{m1i} and θ_{m2i} decrease) are included. However, non-monotonic solutions can still be acquired based on (5). For instance, referring to Fig. 5(b), the $(\theta_{m1i}, \theta_{m2i})$ curve with $40\Omega \le Z_{mi} \le 100\Omega$ under $R_S = 10\Omega$ shows non-monotonicity. Thus, only the results corresponding to $Z_{mi} = 40$, 50 Ω are exhibited in Fig. 6 to avoid the intersection of constant-R_S gridlines.

In addition, using $g_2 = 0.6220$ and $g_3 = 1.3554$ $(Q_{EO} = 12.0443)$, the design graphs for determining the electrical lengths $(\theta_{m1o}, \theta_{m2o})$ of the output Π-tapped feed using both Z_{mo} and $20\ \Omega \le R_L \le 440\ \Omega$ as parameters with selected open-ended stub $(Z_{s2}, \theta_{s2}) = (70\Omega, 30°)$ are shown in Fig 7 Note that the design charts shown in Fig. 6 and Fig. 7 can be flexibly utilized in any center frequency f_0.

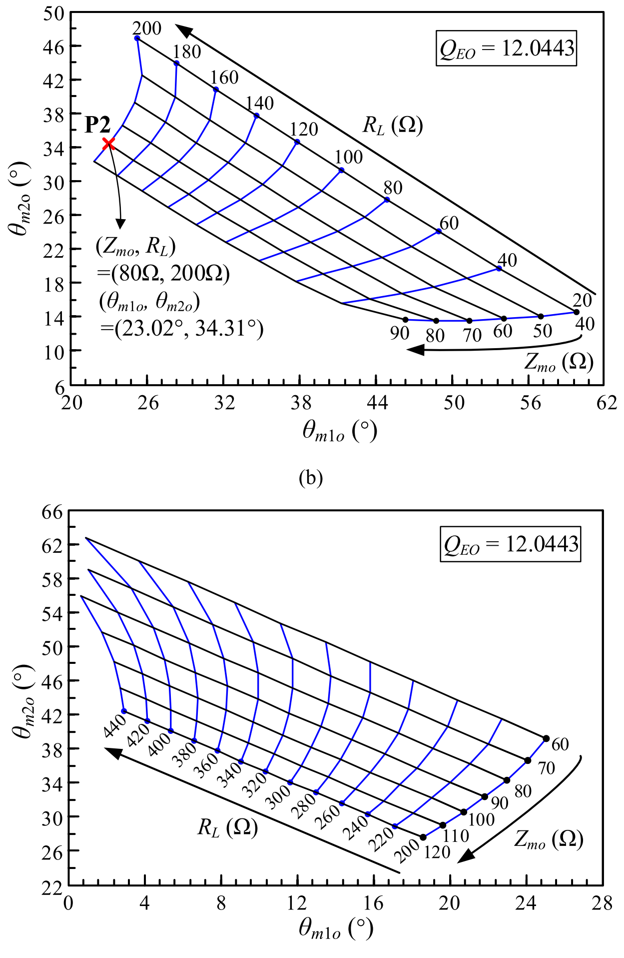

FIGURE 7. Design graph of θ_{m1o} and θ_{m2o} using Z_{mo} and R_L as parameters with termination open-ended stub (Z_{s2}, θ_{s2}) = (70 Ω, 30°). (a) R_L = 20 to 200 Ω. (b) R_L = 200 to 440 Ω.

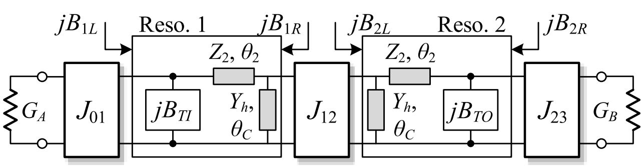

FIGURE 8. Design model for the proposed type-A bandpass.

III. DESIGN OF TYPE-A BPIMT USING A PCL SECTION

In addition to the Π-tapped feeds realizing the specified external quality factor, the SE-PCL section constituting the BPIMT provides the required interstage coupling. On the foundation of Sec. II, the design model of the proposed type-A BPIMT shown in Fig. 2 is depicted in Fig. 8. The design approach of the proposed BPIMT will be investigated in this section.

A. SHORT-ENDED PARALLEL COUPLED-LINE

The SE-PCL serving as the interstage coupling adopted in Fig. 2 for even-/odd-mode characteristic impedances (Z_{0e}, Z_{0o}) and coupled length θ_c can be modeled [26] by an admittance inverter J_{12} attached to two shunt short-circuited stubs (θ_C, Y_h) as shown in Fig. 9. The required J_{12} value is determined by the two adjacent resonators. The input admittances looking toward the LHS and RHS of inverter J_{12} are jB_{1R} and jB_{2L} associated with resonators 1 and 2, respectively, and they can be readily calculated by network analysis. It is worth mentioning that the two resonators are not identical due to asymmetric R_S and R_L, and thus, they possess different susceptance slope parameters observed from the LHS of resonator 1 and from the RHS of resonator 2 given as

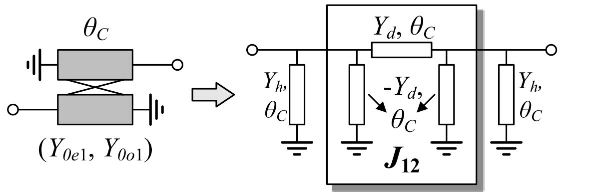

FIGURE 9. Equivalent-circuit model of the SE-PCL adopted in Fig. 2.

$$\begin{aligned} B_{1R} &= -Y_h \cot\theta_C + Y_2(B_{TI} + Y_2\tan\theta_2)\big/(Y_2 - B_{TI}\tan\theta_2) \\ B_{2L} &= -Y_h \cot\theta_C + Y_2(B_{TO} + Y_2\tan\theta_2)\big/(Y_2 - B_{TO}\tan\theta_2) \end{aligned} \tag{6}$$

The susceptance slope parameters b_{1R} and b_{2L} at f_0 can be found by differentiating B_{1R} and B_{2L} with respect to frequency.

By providing the coupled length θ_C, the preferable reference admittance Y_h, and the coupling coefficient k_{12}, the Y_{0e} and Y_{0o} of the PCL section can be solved from

$$Y_{0e} = Y_h + J_{12}\sin\theta_C \text{ and } Y_{0o} = Y_h - J_{12}\sin\theta_C \tag{7a}$$

with $J_{12} = Y_d / \sin\theta_C$ and $Y_h = (Y_{0o} + Y_{0e})/2$. As a result, the admittance inverter value can be obtained through

$$\frac{J_{12}}{\sqrt{b_{1R}b_{2L}}} = k_{12} = \frac{\Delta}{\sqrt{g_1 g_2}}, \text{ where } Y_d = \frac{Y_{0o} - Y_{0e}}{2}. \tag{7b}$$

According to (7), it is evident that both the source and load resistances R_S and R_L will affect the interstage coupling since b_{1R} and b_{2L} depend on source and load terminations, respectively. After determining that the source impedance R_S = 10 Ω, the coupled length θ_c = 70°, the element values of lowpass prototype g_2 = 0.8431, g_3 = 0.6220, and the FBW Δ = 7%, the calculated even-/odd-mode impedances (Z_{0e}, Z_{0o}) with R_L as parameters are drawn in Fig. 10 indicating that the variation of the load resistance alters the even-/odd-mode impedances. Note that for layout convenience, the line characteristic impedances Z_{mo} of the output Π-tapped feed are chosen as 60 Ω for 20 Ω ≤ R_L ≤ 200 Ω and 80 Ω for 200 Ω ≤ R_L ≤ 440 Ω.

B. COMPLETE BANDPASS IMPEDANCE TRANSFORMER DESIGN

The design procedure is as follows:

1) Specify the source and load impedances (R_S, R_L), the filter specifications including f_0, FBW, and the lowpass prototype response thus giving the relevant Q_{EI}, Q_{EO}, and k_{12}.

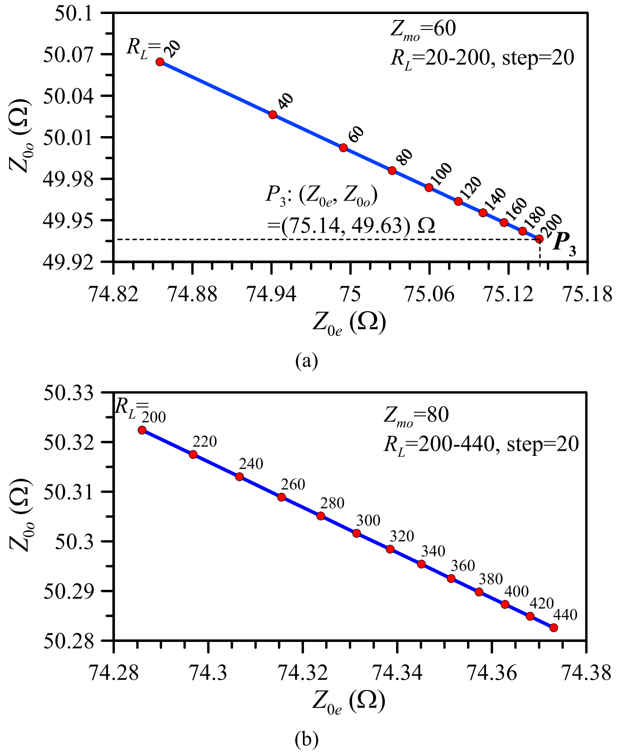

FIGURE 10. Design graph for determining (Z_{0e}, Z_{0o}) using R_L as a parameter with termination $R_S = 10\ \Omega$, open-ended stubs $(Z_{s1}, \theta_{s1}) = (70\ \Omega, 45°)$ and $(Z_{s2}, \theta_{s2}) = (70\Omega, 30°)$, coupled length $\theta_C = 70°$, the reference impedance $Z_h = 60\ \Omega$, and $Z_2 = 60\ \Omega$ (the filter is designed for Chebyshev 0.1-dB-ripple response). (a) $20\ \Omega \le R_L \le 200\ \Omega$. (b) $200\ \Omega \le R_L \le 440\ \Omega$.

2) Determine the impedance values Z_1 and Z_2 of the $\lambda/4$ SIR and calculate the corresponding susceptance slope parameter $b_{\lambda/4}$.
3) Select the appropriate characteristic impedances Z_{mi} and Z_{mo} for the I/O Π-tapped feeds and pick up the open-circuited stubs (Z_{s1}, θ_{s1}) and (Z_{s2}, θ_{s2}). The electrical lengths (θ_{m1} and θ_{m2}) can then be calculated based on (5). The auxiliary design graphs for determining the electrical lengths θ_{m1} and θ_{m2} relevant to the input and output feeds can be drawn to facilitate the design.
4) Once the I/O Π-tapped feeds are both available, the susceptance slope parameters b_{1R} and b_{2L} required in (7) for obtaining the even-/odd-mode impedances of the PCL section can be calculated by (6). The auxiliary design graphs for determining the PCL impedances Z_{0e} and Z_{0o} can be drawn to facilitate the design.
5) Finally, convert the electrical design parameters into physical dimensions and optimize the BPIMT using a full-wave EM simulator.

Note that the asymmetric structure makes the high impedance transformation ratio possible and the synthesis approach is applicable for flexible r_Z. Different from those works in the literature, the proposed approach originated from the inverter-based coupled-resonator filter.

TABLE 1. Circuit design parameters.

	Design parameters ($Z_1 = Z_2 = 60\ \Omega$)
CktA1 (10:200)	f_0 = 2.5 GHz, ripple-FBW=7% (theoretical 3 dB-FBW = 13.56%) Chebyshev 0.1-dB-ripple response θ_{m1i} = 44.19º, θ_{m2i} = 11.69º, θ_{m1o} = 25.08º, θ_{m2o} = 39.19º, θ_2 = 20º, Z_{mi} = 60 Ω, Z_{mo} = 60 Ω, θ_C = 70º, (Z_{0e}, Z_{0o}) = (74.699, 50.1347) Ω
CktA2 (5:475)	f_0 = 2.0 GHz, 3 dB-FBW=7% Butterworth response θ_{m1i} = 52.25º, θ_{m2i} = 14.97º, θ_{m1o} = 4.05º, θ_{m2o} = 52.6º, θ_2 = 20º, Z_{mi} = 50 Ω, Z_{mo} = 80 Ω, θ_C = 70º, (Z_{0e}, Z_{0o}) = (70.0033, 52.4982) Ω

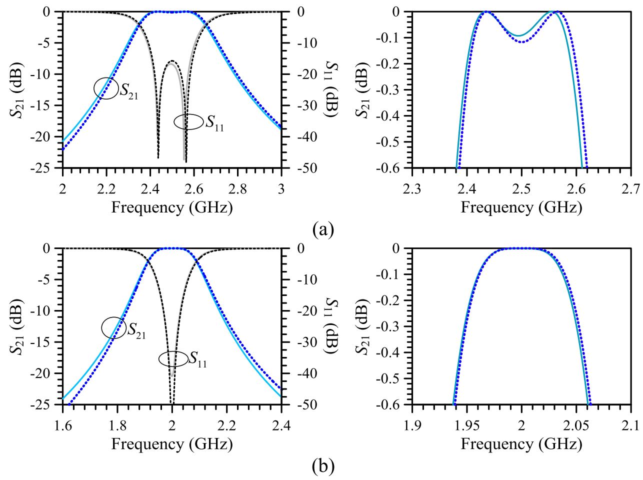

FIGURE 11. Circuit-level simulated (solid line) scattering and calculated parameters from the coupling-matrix analysis (dashed line) of BPIMTs CktA1 and CktA2. (a) 10:200 Chebyshev 0.1-dB-ripple response FBW=7%. (b) 5:475 Butterworth response FBW = 10%.

IV. DESIGN AND IMPLEMENTATION OF A TYPE-A BPIMT

To demonstrate the synthesis feasibility, two sample circuits with the specifications shown in Table 1 are designed. CktA1 is designed with a moderate transforming ratio of $r_Z = 20\ \Omega/\Omega$ whereas CktA2 is designed with an extremely high impedance ratio of $r_Z = 95\ \Omega/\Omega$. The circuit-level simulated results using ideal TL components and the calculated results from coupling-matrix analysis are compared in Fig. 17 showing satisfactory agreement in terms of bandwidth, return loss, and passband ripple. The design formulas are proven accurate for achieving a target filtering impedance transformer.

The two type-A BPIMTs will be fabricated and measured in this section. The measurements are carried out by an R&S ZVB20 network analyzer. For measurement purposes, two 15-mm-long 50 Ohm lines are attached to the I/O ports of all circuits where the TRL (through-reflection-line) calibration technique is then adopted to de-embed their effects including the SMA connectors.

A. BPIMT CKTA1: $r_Z = 20$

A sample BPIMT (CktA1) with $R_S = 10\ \Omega$ and $R_L = 200\ \Omega$ was designed with $f_0 = 2.5$ GHz and ripple-$\Delta = 7\%$

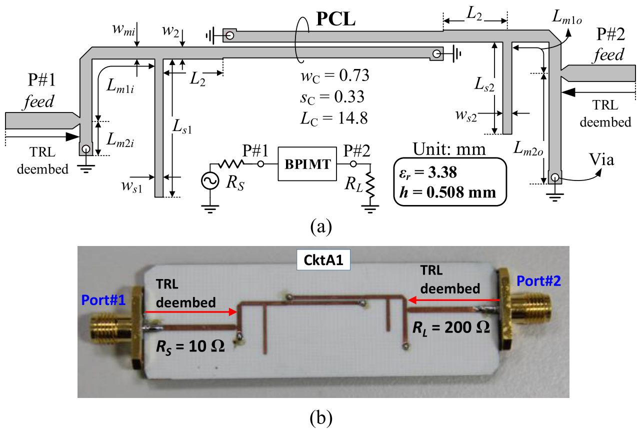

FIGURE 12. (a) Layout ($w_m = 0.81$, $L_{m1i} = 8.7$, $L_{m2i} = 2.3$, $w_2 = 4.3$, $L_2 = 0.81$, $w_{s1} = 0.57$, $L_{s1} = 9.3$, $w_{s2} = 0.57$, $L_{s2} = 6.2$, $L_{m1o} = 4.9$, $L_{m2o} = 7.45$ mm) and (b) circuit photograph of the proposed bandpass impedance transformer CktA1 (10:200).

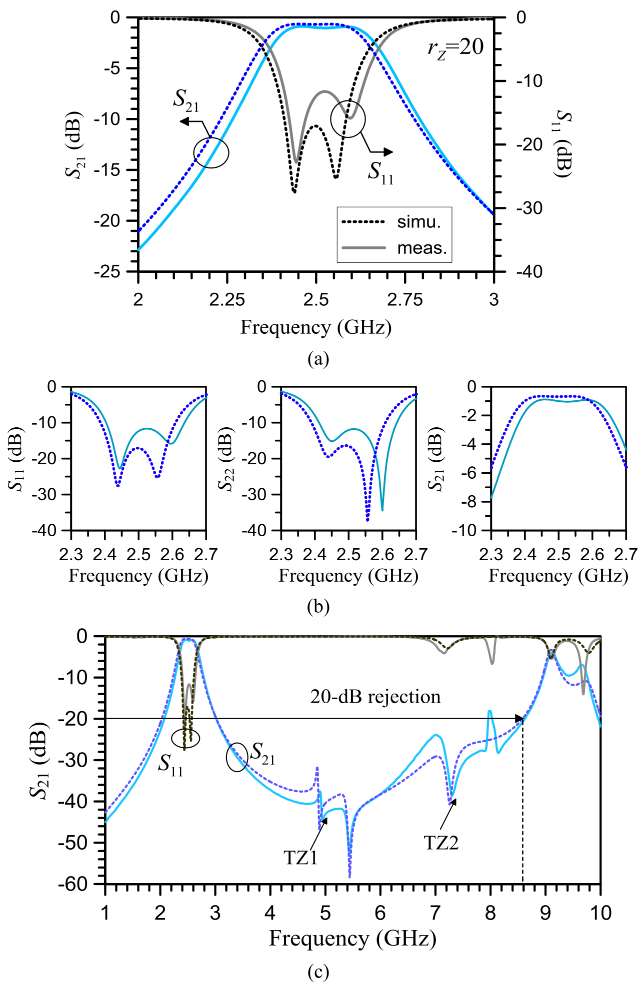

FIGURE 13. EM simulated and measured scattering parameters of the 10:200 BPIMT CktA1 with Chebyshev 0.1-dB-ripple response and FBW=7%. (a) Passband S_{11} and S_{21}. (b) Zoom-in S_{11}, S_{22}, and S_{21}. (c) Wideband-view response.

for a Chebyshev 0.1-dB-ripple response. The filter design parameters are $Q_{EI} = Q_{EO} = 12.044$ and $k_{12} = 0.0967$. The $\lambda/4$ SIR has $Z_1 = Z_2 = 60\ \Omega$, $\theta_c = 70°$, $\theta_2 = 20°$ and its relevant $b_{\lambda/4} = 1.31$ cS. The two open-circuited stubs attached to the input and output tapped feeds are picked up with electrical lengths 45° and 30°, respectively, for creating TZs at $2f_0$ and $3f_0$. With (3), the calculated susceptance slope parameters are $(b_{1L}, b_{2R}) = (35.23, 29.4)$ cS. The calculated electrical length $(\theta_{m1i}, \theta_{m2i})$ of the input tapped feed with $Z_{mi} = 60\ \Omega$ is labeled point P1 in Fig. 6 whereas the $(\theta_{m1o}, \theta_{m2o})$ of the output tapped feed with $Z_{MO} = 60\ \Omega$ is labeled point P2 in Fig. 7. With (6), the $(b_{TI}, b_{TO}) = (22.14, 16.31)$ cS and $(b_{1R}, b_{2L}) = (39.56, 32.95)$ cS leading to the inverter value $J_{12} = 3.49$ cS. By setting $Z_{mo} = Z_{mi}$, point P3 in Fig. 10 gives the PCL information. The design electrical parameters for the schematic of the type-A BPIMT in Fig. 2 are now completely determined.

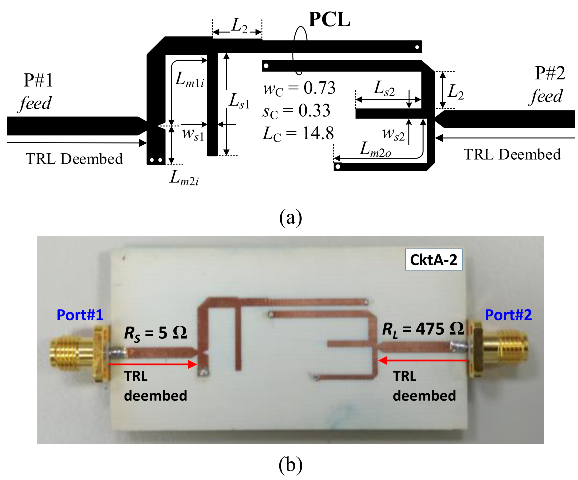

FIGURE 14. (a) Layout ($w_{mi} = 1.9$, $L_{m1i} = 9.55$, $L_{m2i} = 4.1$, $w_2 = 1.45$, $L_2 = 5.3$, $w_{s1} = 1.1$, $L_{s1} = 11.8$, $w_{s2} = 1.1$, $L_{s2} = 8.1$, $w_{mo} = 0.86$, $L_{m2o} = 15.1$) and (b) circuit photograph of the proposed bandpass impedance transformer CktA2 (5:475).

The transformer CktA1 was implemented on a 0.508-mm-thick RO4003c substrate ($\varepsilon_r = 3.55$, $\tan\delta = 0.0027$). The layout dimensions of the fabricated BMIMT CktA1 are annotated in Fig. 14. The circuit size excluding the feedlines is 32.32×10.36 mm^2 ($0.2265 \times 0.085\ \lambda_0^2$). The passband scattering parameters are shown in Fig. 15(a) and the zoom-in S_{11}, S_{22}, and S_{21} are presented in Fig. 15(b). The measured center frequency, minimum insertion loss and 3 dB-FBW are 2.52 GHz, 0.883 dB and 13.26%, respectively. The −10-dB return loss bandwidth is from 2.404 to 2.636 GHz. The wideband frequency response ranging from 1 to 10 GHz is shown in Fig. 15(c). The 20 dB rejection bandwidths at lower and higher sidebands are from dc to 2.074 GHz and from 3.02 to 8.62 GHz. Note that the abrupt spike approximately 8 GHz may result from the inaccuracy of the TRL calibration.

B. BPIMT CKTA2: $r_Z = 95$

The other type-A BPIMT (CktA2) with much higher impedance ratio $r_Z = 95$ (5:475) is demonstrated. The transformer is designed with $f_0 = 2.0$ GHz and 3 dB-Δ = 10%

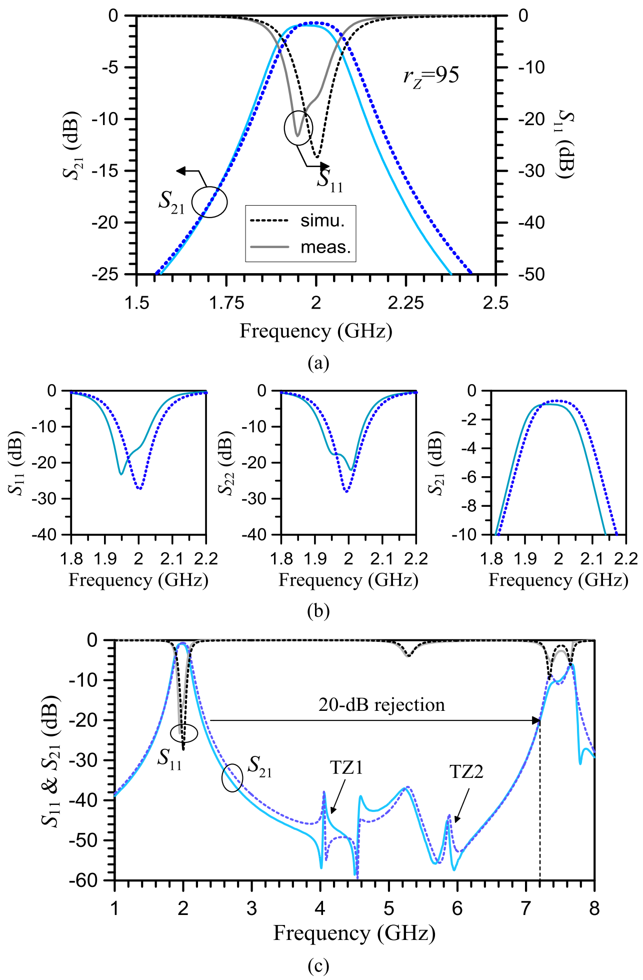

FIGURE 15. EM simulated and measured inband scattering parameters of the BPIMT CktA2 (5:475) with Butterworth response FBW=10%. (a) Passband S_{11} and S_{21}. (b) Zoom-in S_{11}, S_{22}, and S_{21}. (c) Wideband-view response.

for a Butterworth response. The filter design parameters are $Q_{\mathrm{EI}} = Q_{\mathrm{EO}} = 14.14$ and $k_{12} = 0.0707$. It is worth mentioning that since the filter response is chosen differently now, the deign graphs for finding the $(\theta_{m1}, \theta_{m2})$ of the input/output Π-tapped feeds and the $(Z_{0\mathrm{e}}, Z_{0\mathrm{o}})$ shown in Figs. 6, 7, and 10 can be re-drawn on the derived formulas (5) and (7) if required.

A λ/4 SIR identical to CktA1 is also selected here. The calculated susceptance slope parameters are $(b_{1L}, b_{2R}) = (37.58, 26.92)$ cS and $(b_{1R}, b_{2L}) = (42.34, 30.34)$ cS available for calculation of the model parameters. The electrical lengths for the input and output tapped feeds are $(\theta_{m1i}, \theta_{m2i}) = (52.25°, 14.97°)$ with $Z_{mi} = 50\ \Omega$ and $(\theta_{m1o}, \theta_{m2o}) = (4.05°, 52.6°)$ with $Z_{mo} = 80\ \Omega$, respectively. The inverter value J_{12} is 2.534 cS resulting in $(Z_{0\mathrm{e}}, Z_{0\mathrm{o}}) = (70.0033, 52.4982)\ \Omega$ with $\theta_C = 70°$ and $Z_h = 60\ \Omega$.

The transformer is implemented on an 0.813-mm-thick RO4003c substrate ($\varepsilon_{\mathrm{r}} = 3.55$, $\tan\delta = 0.0027$). The layout dimensions of the fabricated BMIMT CktA2 are annotated in Fig. 12. The circuit size excluding the feedlines is 30.85 × 14.37 mm^2 (0.203 × 0.095 λ_0^2). The passband scattering parameters are shown in Fig. 13(a) and the zoom-in S_{11}, S_{22}, and S_{21} are presented in Fig. 13(b). The measured center frequency, minimum insertion loss and 3 dB-FBW are 1.974 GHz, 0.9436 dB and 10.033%, respectively. The −10-dB return loss bandwidth is from 1.913 to 2.034 GHz. The wideband frequency response ranging from 1 to 8 GHz is shown in Fig. 13(c). The 20-dB rejection bandwidths at lower and higher sidebands are from dc to 1.67 GHz and from 2.275 to 7.2 GHz. Two transmission zeros, TZ1 and TZ2 contributed by the open-circuited stubs, can be found among the stopband.

V. DESIGN AND IMPLEMENTATION OF THE TYPE-B BPIMT USING INDUCTIVE COUPLING

The impedance-transformation technique based on the proposed Π-tapped feeds can be applied in different types of coupled-resonator filter topologies. Different from the type-A BPIMT, in this section, the type-B BPIMT utilizing inductive coupling [27] is proposed as shown in Fig. 16(a).

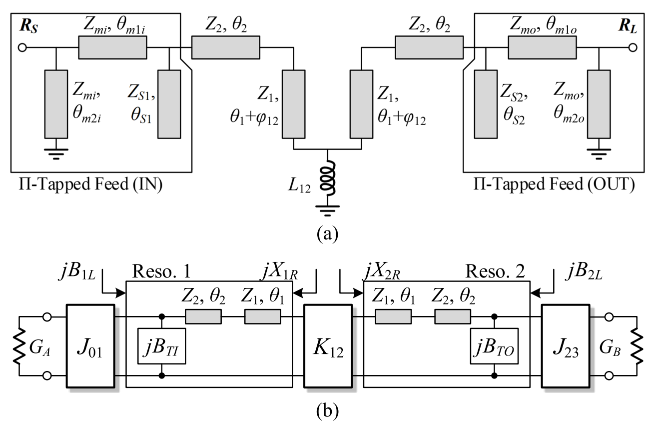

FIGURE 16. Type-B BPIMT with inductive coupling. (a) Schematic. (b) Inverter-based equivalent-circuit model.

A. DESIGN APPROACH

The schematic shown in Fig. 16(a) can be converted to the equivalent-circuit model presented in Fig. 16(b). Likewise, the Π-tapped feed can be design based on Sec. II. For the inductive coupling between resonators [28], it can be modeled as an impedance inverter K_{12}

$$L_{12} = \frac{Z_1}{\omega_0}\frac{K_{12}/Z_1}{1-(K_{12}/^2} \quad \text{and} \quad \varphi_{12} = -\frac{1}{2}\tan^{-1}\frac{2X_{12}}{Z_1}. \tag{8a}$$

with

$$K_{12} = \sqrt{\frac{\Delta^2 \cdot x_{1R} \cdot x_{2L}}{g_1 g_2}}, \tag{8b}$$

where $x_{1\mathrm{R}}$ and $x_{2\mathrm{L}}$ are the reactance slope parameters observed from the LHS of resonator 1 and from the RHS of resonator 2, respectively. The reactance slope parameters $x_{1\mathrm{R}}$ and $x_{2\mathrm{L}}$ at f_0 can be found by differentiating $X_{1\mathrm{R}}$ and $X_{2\mathrm{L}}$ with respect to frequency. The reactances $X_{1\mathrm{R}}$ and $X_{2\mathrm{L}}$ are

$$X_{1R} = \frac{(B_{TI}\tan\theta_2 - Y_2) + \alpha_Y \tan\theta_1 (B_{TI} + Y_2\tan\theta_2)}{\alpha_Y^{-1}(Y_2 - B_{TI}\tan\theta_2) + (B_{TI} + Y_2\tan\theta_2)}$$
$$X_{2L} = \frac{(B_{TO}\tan\theta_2 - Y_2) + \alpha_Y \tan\theta_1 (B_{TO} + Y_2\tan\theta_2)}{\alpha_Y^{-1}(Y_2 - B_{TO}\tan\theta_2) + (B_{TO} + Y_2\tan\theta_2)}. \tag{9}$$

Note that under the particular UIR condition, the TL section $\theta_1 + \theta_2$ becomes a uniform $\lambda/4$ transformer with characteristic admittance $Y_1(= 1/Z_1)$ at f_0 causing

$$X_{1R} \approx B_{TI}/Y_1^2 \text{ and } X_{2L} \approx B_{TO}/Y_1^2. \tag{10a}$$

Based on (10a), the x_{1R} and x_{2L} are approximated as

$$x_{1R} \approx b_{TI}/Y_1^2 \text{ and } x_{2L} \approx b_{TO}/Y_1^2 \tag{10b}$$

where b_{TI} and b_{TO} represent the susceptance slope parameters of the input and output Π-tapped feeds. Through (10), one can convert the calculated b_{TI} and b_{TO} acquired from (5) to the $x_{1\mathrm{R}}$ and $x_{2\mathrm{L}}$ required in (8) for this type-B BPMIT as the target FBW is relatively narrow.

For demonstration, a BPIMT with $f_0 = 2.0$ GHz and 3 dB-$\Delta = 10\%$ was designed for a Butterworth response. The filter design parameters are $Q_{EI} = Q_{EO} = 12.044$ and $k_{12} = 0.0967$. The line impedances $Z_{mi} = 50\ \Omega$ and $Z_{mo} = 80\ \Omega$ for the input/output Π-tapped feeds are first determined, and the $\lambda/4$ SIRs adopted here are $Z_1 = Z_2 = 60\ \Omega$ and $\theta_1 + \theta_2 = 90°$. The calculated susceptance slope parameters are $(b_{\mathrm{TI}}, b_{\mathrm{TO}}) = (24.49, 13.84)$ cS, $(b_{1L}, b_{2R}) = (37.58, 26.93)$ cS, and $(x_{1R}, x_{2L}) = (134.08, 96.35)\ \Omega$ for evaluating the model parameters. The electrical lengths for the input and output Π-tapped feeds are $(\theta_{m1i}, \theta_{m2i}) = (52.25°, 14.97°)$ and $(\theta_{m1o}, \theta_{m2o}) = (0.41°, 56.18°)$, respectively. The inverter value K_{12} is 8.038 Ω resulting in $L_{12} = 0.6513$ nH with $\varphi_{12} = -7.63°$. The circuit-level simulated results using ideal TL components and the calculated results from the coupling-matrix analysis are compared in Fig. 17, showing significant agreement in terms of bandwidth, return loss, and passband ripple.

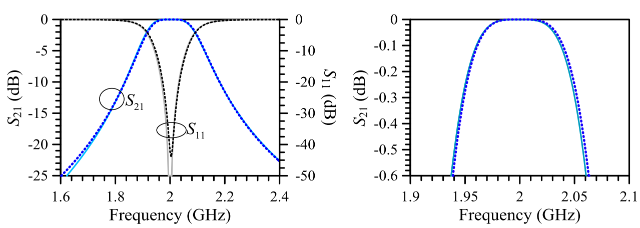

FIGURE 17. Circuit-level simulated (solid line) scattering and calculated parameters from the coupling-matrix analysis (dashed line) of the 5:520 BPIMT CktB with Butterworth response FBW = 10%.

In microwave practice, short-ended stubs are commonly adopted to implement the inductive components. To reduce the effect of process tolerance, a double-loaded short-circuited stub is employed to achieve the required $K_{12} = 8.03813\ \Omega$. The inverter value K_{12} and electrical lengths of the cascading lines corresponding to the inductive coupling can be extracted with the EM simulator [29]. The EM-extracted inverter values vs. frequency are shown in Fig. 18(a). The realistic K_{12} / φ_{12} design graph extracted at 2 GHz vs. the stub length l_{in} is displayed in Fig. 18(b). With the aid of Fig. 18(b), one can determine the demanded stub length according to the filter specification.

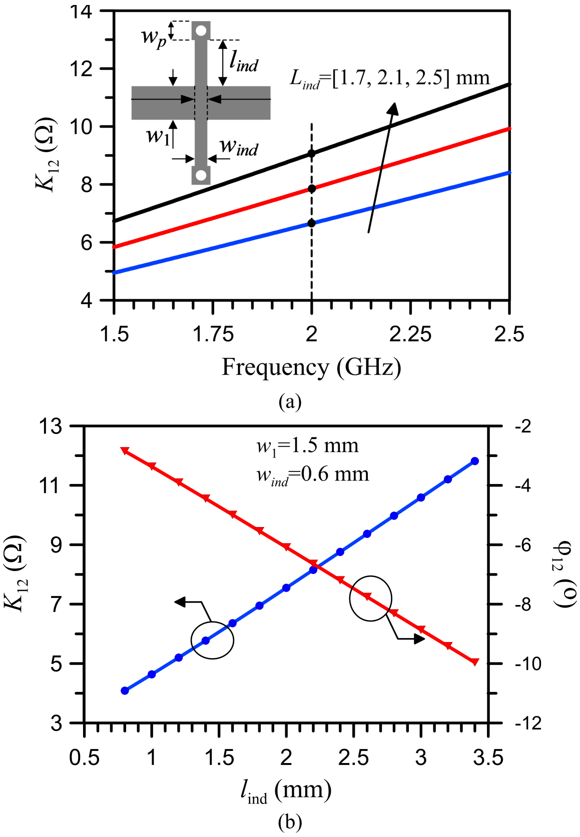

FIGURE 18. EM-extracted inverter K_{12} value ($w_1 = 1.5$, $w_{\mathrm{ind}} = 0.6$, $w_p = 0.9$ mm, Via diameter = 0.5 mm). (a) K_{12} vs. frequency. (b) Design graphs of K_{12} / φ_{12} vs. d_{12} @ $f_0 = 2$ GHz.

B. IMPLEMENTATION AND MEASUREMENT

The transformer CktB was fabricated on an 0.813-mm-thick RO4003c substrate ($\varepsilon_{\mathrm{r}} = 3.55$, $\tan\delta = 0.0027$). The layout dimensions of the fabricated BMIMT CktB are annotated in Fig. 19. The circuit size excluding the feedlines is 31.22×23.5 mm^2 ($0.208 \times 0.156\ \lambda_0^2$). The passband scattering parameters are shown in Fig. 20(a) and the zoom-in S_{11}, S_{22}, and S_{21} vs. frequency are presented in Fig. 20(b). The measured center frequency, minimum insertion loss and 3 dB-FBW are 1.997 GHz, 1.171 dB and 7.96%, respectively. The -10-dB S_{11} and S_{22} bandwidths are 1.96-2.048 and 1.958-2.067 GHz, respectively. The measured bandwidth shrinkage may result from the drilling inaccuracy of the hole position. The wideband frequency response ranging from 1 to 8 GHz is shown in Fig. 20(c). The 20-dB rejection bandwidths at lower and higher sidebands are from dc to 1.771 GHz and from 2.266 to 4.497 GHz. Since the resonators

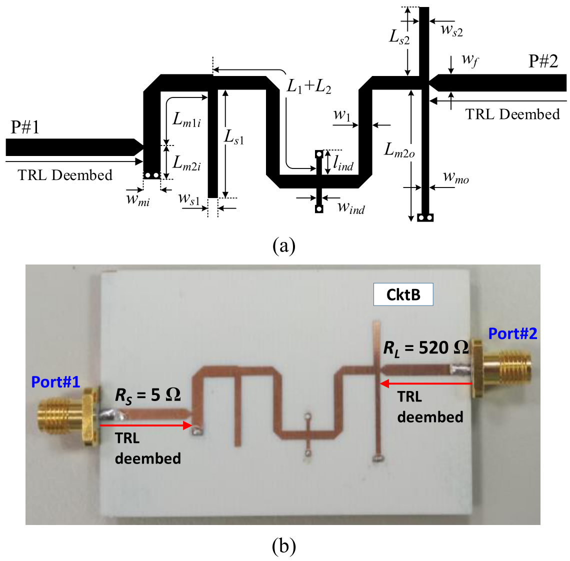

FIGURE 19. **(a) Layout ($w_f = 1.9$, $w_{MI} = 1.9$, $L_{m1i} = 11.63$, $L_{m2i} = 3.49$, $w_{s1} = 1.1$, $L_{s1} = 11.65$, $w_1 = 1.5$, $L_1 + L_2 = 18.55$, $w_{ind} = 0.6$, $l_{ind} = 2.13$, $w_{mo} = 0.83$, $L_{m2o} = 14.45$, $w_{s2} = 1.1$, $L_{s2} = 7.5$, Unit: mm) and (b) circuit photograph of the proposed bandpass impedance transformer CktB (5:520).**

constituting the BPIMT are linked by inductive coupling, the resonance phenomena become more complicated than the edge-coupled type filter. The out-of-band response cannot merely be predicted by the isolated resonator resonances but by the resonances of linked resonators.

TABLE 2. **Comparison with previous works.**

Ref	f_c (GHz)	FBW (%)	Ratio r_Z (Ω/Ω)	Specification Designable
[10]	2.0	77.8% (17 dB RL)	$r_z = 2.2$ (50:110)	FBW (yes) response (yes)
[12]	2.0	54% (15 dB RL)	$r_z = 4.0$ (50:200)	FBW (no) Response (yes)
[15]	2.0	13.22 (15 dB RL)	$r_z = 2.0$ (25:50)	FBW (yes) response (yes)
[17]	1.0	50% (15 dB RL)	$r_z = 2.0$ (25:50)	FBW (yes) response (yes)
[18]	2.0	9.6% (15 dB RL)	$r_z = 20$ (50:1000)	FBW (yes) response (yes)
[19]	2.6	8.27% (18 dB RL)	$r_z = 10$ (5:50)	FBW (yes) response (yes)
This CktA1	2.5	Chebyshev 13% (3 dB-IL)	$r_Z = 20$ (10:200)	FBW (yes) response (yes)
This CktA2	2.0	Butterworth 10% (3 dB-IL)	$r_Z = 95$ (5:475)	FBW (yes) response (yes)
This CktB	2.0	Butterworth 10% (3 dB-IL)	$r_Z = 104$ (5:520)	FBW (yes) response (yes)

* IL: insertion loss; RL: return loss

VI. PERFORMANCE COMPARISON AND DISCUSSION

Table 2 compares the three circuits proposed in this study with filtering impedance transformers in the literature. The proposed BPIMT utilizing Π-tapped feeds originates from the inverter-based coupled-resonator filter and thus can be designed through the external quality factors and coupling coefficients according to specifications. In this way, as the filtering order goes higher, the design approach can be readily extended without increasing complexity too much. The filter response and FBW can be more flexibly controlled. It is worth mentioning that the proposed BPIMTs achieve an extremely high impedance transforming ratio and a wide range of source and load impedances.

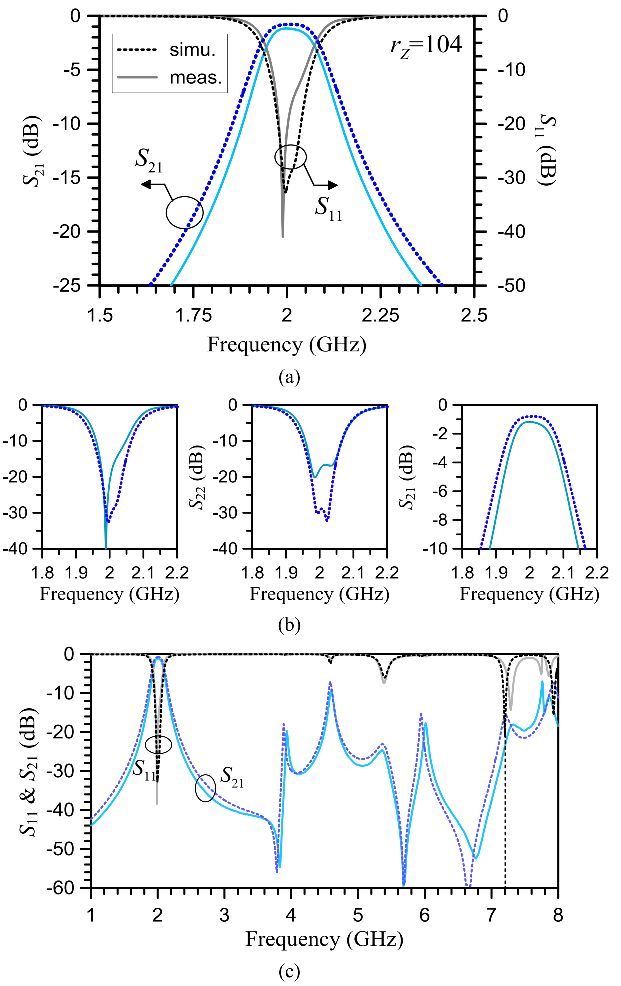

FIGURE 20. **EM simulated and measured inband scattering parameters S_{11} and S_{21} of the 5:520 BPIMT CktB with Butterworth response FBW=10%. (a) Passband S_{11} and S_{21}. (b) Zoom-in S_{11}, S_{22}, and S_{21}. (c) Wideband-view response.**

VII. CONCLUSION

Bandpass impedance transformers featuring extremely high transforming ratio, designable filter response, and simple structure are proposed in this study. The synthesis approaches, detailed design formulas and the auxiliary design graphs for two different BPIMT topologies are well developed and validated by experimental results. Theoretically speaking, the proposed Π-tapped feeds can be extensively applied in most coupled-resonator filters for achieving impedance transformation. Moreover, the synthesis method can be readily extended to BPIMT with higher order ($N > 2$). Specifically, the proposed BPIMTs achieve an extremely high transforming ratio of 104, which is the highest value reported to the best of the authors' knowledge. The BPIMT can find applications in RF/microwave front ends.

ACKNOWLEDGMENT

The authors would like to thank National Center for High-Performance Computing (NCHC) of National Applied Research Laboratories (NARLabs) of Taiwan for providing computational resources and storage resources.

REFERENCES

[1] S. Gruszczynski and K. Wincza, "Broadband rat-race couplers with coupled-line section and impedance transformers," *IEEE Microw. Compon. Lett.*, vol. 22, no. 1, pp. 22–24, Jan. 2012.

[2] H. R. Ahn and I. Wolff, "General design equations, small-sized impedance transformers, and their application to small-sized three-port 3-dB power dividers," *IEEE Trans. Microw. Theory Techn.*, vol. 49, no. 7, pp. 1277–1288, Jul. 2001.

[3] S. Lee and Y. Lee, "Wideband branch-line couplers with single-section quarter-wave transformers for arbitrary coupling levels," *IEEE Microw. Wireless Compon. Lett.*, vol. 22, no. 1, pp. 19–21, Jan. 2012.

[4] C.-H. Huang, T.-S. Horng, C.-C. Wang, C.-T. Chiu, and C.-P. Hung, "Optimum design of transformer-type Marchand balun using scalable integrated passive device technology," *IEEE Trans. Compon., Packag., Manuf. Technol.*, vol. 2, no. 8, pp. 1370–1377, Aug. 2012.

[5] J. Shao, R. Zhou, C. Chen, X.-H. Wang, H. Kim, and H. Zhang, "Design of a wideband balun using parallel strips," *IEEE Microw. Wireless Compon. Lett.*, vol. 23, no. 3, pp. 125–127, Mar. 2013.

[6] M. Abbasi, H. Zirath, and I. Angelov, "Q-, V-, and W-band power amplifiers utilizing coupled lines for impedance matching," in *IEEE MTT-S Int. Microw. Symp. Dig.*, Jun. 2008, pp. 863–866.

[7] V. Radisic, Y. Qian, and T. Itoh, "Novel architectures for high-efficiency amplifiers for wireless applications," *IEEE Trans. Microw. Theory Techn.*, vol. 46, no. 11, pp. 1901–1909, Nov. 1998.

[8] X. H. Fang and K. K. M. Cheng, "Improving power utilization factor of broadband doherty amplifier by using bandpass auxiliary transformer," *IEEE Trans. Microw. Theory Techn.*, vol. 63, no. 9, pp. 2811–2820, Sep. 2015.

[9] W. J. Lu, K. S. Ang, and K. Mouthaan, "A broadband quarter-wavelength impedance transformer using vertically installed planar coupler," in *IEEE MTT-S Int. Microw. Symp. Dig.*, Jun. 2011, pp. 1–4.

[10] Q.-S. Wu and L. Zhu, "Wideband impedance transformers with good frequency selectivity based on multisection quarter-wave lines and short-circuited stubs," *IEEE Microw. Wireless Compon. Lett.*, vol. 26, no. 5, pp. 337–339, May 2016.

[11] S. B. Cohn, "Optimum design of stepped transmission-line transformers," *IRE Trans. Microw. Theory Techn.*, vol. 3, no. 3, pp. 16–20, Apr. 1955.

[12] R. Darraji, M. M. Honari, R. Mirzavand, F. M. Ghannouchi, and P. Mousavi, "Wideband two-section impedance transformer with flat real-to-real impedance matching," *IEEE Microw. Wireless Compon. Lett.*, vol. 26, no. 5, pp. 313–315, May 2016.

[13] E. Rotholz, "Transmission-line transformers," *IEEE Trans. Microw. Theory Techn.*, vol. TMTT-29, no. 4, pp. 327–331, Apr. 1981.

[14] N. Ehsan, W.-T. Hsieh, S. H. Moseley, and E. J. Wollack, "Broadband planar 5:1 impedance transformer," *IEEE Microw. Wireless Compon. Lett.*, vol. 25, no. 10, pp. 636–638, Oct. 2015.

[15] H.-R. Ahn and T. Itoh, "Impedance-transforming symmetric and asymmetric DC blocks," *IEEE Trans. Microw. Theory Techn.*, vol. 58, no. 9, pp. 2463–2474, Sep. 2010.

[16] A. Podcameni, "Symmetrical and asymmetrical edge-coupled-line impedance transformers with a prescribed insertion loss design," *IEEE Trans. Microw. Theory Techn.*, vol. TMTT-34, no. 1, pp. 1–6, Jan. 1986.

[17] Q. Wu and L. Zhu, "Synthesis design of a wideband impedance transformer consisting of two-section coupled lines," *IET Microw., Antennas Propag.*, vol. 11, no. 1, pp. 144–150, Jan. 2017.

[18] Q.-S. Wu and L. Zhu, "Short-ended coupled-line impedance transformers with ultrahigh transforming ratio and bandpass selectivity suitable for large load impedances," *IEEE Trans. Compon. Packag. Manuf. Technol.*, vol. 6, no. 5, pp. 767–774, May 2016.

[19] P. Kim, G. Chaudhary, and Y. Jeong, "Ultra-high transforming ratio coupled line impedance transformer with bandpass response," *IEEE Microw. Wireless Compon. Lett.*, vol. 25, no. 7, pp. 445–447, Jul. 2015.

[20] J. S. Wong, "Microstrip tapped-line filter design," *IEEE Trans. Microw. Theory Techn.*, vol. TMTT-27, no. 1, pp. 44–50, Jan. 1979.

[21] C.-M. Tsai, S.-Y. Lee, and C.-C. Tsai, "Performance of a planar filter using a 0° feed structure," *IEEE Trans. Microw. Theory Techn.*, vol. 50, no. 10, pp. 2362–2367, Oct. 2002.

[22] J. T. Kuo and E. Shih, "Microstrip stepped impedance resonator bandpass filter with an extended optimal rejection bandwidth," *IEEE Trans. Microw. Theory Techn.*, vol. 51, no. 5, pp. 1554–1559, May 2003.

[23] K. Ma, J.-G. Ma, K. S. Yeo, and A. V. Do, "A compact size coupling controllable filter with separate electric and magnetic coupling paths," *IEEE Trans. Microw. Theory Techn.*, vol. 54, no. 3, pp. 1113–1119, Mar. 2006.

[24] C. M. Tsai and H. M. Lee, "Improved design equations of the tapped-line structure for coupled-line filters," *IEEE Microw. Wireless Compon. Lett.*, vol. 17, no. 4, pp. 244–246, Apr. 2007.

[25] S. C. Lin, "Coupled-line filters with stub-embedded resonators using accurate admittance-transformer feeds for flexible terminations," *IEEE Trans. Microw. Theory Techn.*, vol. 62, no. 12, pp. 2911–2922, Dec. 2014.

[26] G. Matthaei, E. M. T. Jones, and L. Young, *Microwave Filters, Impedance-Matching Networks, and Coupling Structures*. Dedham, MA, USA: Artech House, 1980.

[27] C.-H. Wang, Y.-S. Lin, and C. H. Chen, "Novel inductance-incorporated microstrip coupled-line bandpass filters with two attenuation poles," in *IEEE MTT-S Int. Microw. Symp. Dig.*, vol. 3, Jun. 2004, pp. 1979–1982.

[28] D. M. Pozar, *Microwave Engineering*, 4th ed. New York, NY, USA: Wiley, 2011.

[29] S.-C. Lin, "Microstrip dual/quad-band filters with coupled lines and quasi-lumped impedance inverters based on parallel-path transmission," *IEEE Trans. Microw. Theory Techn.*, vol. 59, no. 8, pp. 1937–1946, Aug. 2011.

CHI-WEN HSIEH received the B.Sc. and Ph.D. degrees in electronic engineering from National Tsing-Hua University, Hsinchu, Taiwan, in 1993 and 2007, respectively. Since 2009, he has been with the Department of Electrical Engineering, National Chiayi University, Chiayi, Taiwan, where he is currently an Associate Professor. His research interests include imaging reconstruction for proton therapy, medical imaging processing, and numerical analysis for antenna design.

SHIH-CHENG LIN received the B.S. degree in electrical engineering from National Sun Yat-sen University, Kaohsiung, Taiwan, in 2003, and the Ph.D. degree in communication engineering from National Taiwan University, Taipei, Taiwan, in 2007. In 2007, he joined Taiwan Semiconductor Manufacturing Company, Hsinchu, Taiwan, as an RF-Modeling Engineer. In 2008, he joined Sunplus Technology Company Ltd., Hsinchu, as an Advanced Engineer, where he was involved in the RF integrated circuit design. Since 2009, he has been with the Department of Electrical Engineering, National Chiayi University, Chiayi, Taiwan, where he is currently a Professor. His research interests include the development and design of microwave passive components, RF/microwave integrated circuits, and phased array antennas.

JIA-YING LI received the B.Sc. degree in electrical engineering from National Chiayi University, Chiayi, Taiwan, in 2016, where she is currently pursuing the M.Sc. degree in electrical engineering. Her current research interests include RF/microwave circuits.